Batteries & Supercaps

Research Article
doi.org/10.1002/batt.202300551

Chemistry Europe
European Chemical Societies Publishing

www.batteries-supercaps.org

A Data-Driven Method based on Discrete Wavelet Transform for online Li-Ion Battery State-of-Health Prediction and Monitoring

Dario Pelosi,[a] Federico Gallorini,[b] Panfilo Andrea Ottaviano,[b] and Linda Barelli*[a]

Transportation electrification is accelerating the clean energy transition. Due to high efficiencies and energy density, Li-ion batteries (LIBs) are used as on-board energy carrier for battery electric vehicles (BEVs). LIBs are subject to rapid degradation due to fast-charging, mechanical, electrical and thermal factors. Thus, state-of-health (SoH) prediction is required to optimize LIBs exploitation over their lifespan. An online accurate and easy-of-implementation battery SoH prediction and monitoring method for BEV applications is here presented. The method implements discrete wavelet transform (DWT) analysis to voltage profiles, measured while driving. Specifically, an extensive cycle aging experimental campaign on NCR 18650 cells was performed, applying two typical US test drives (urban and extra-urban drive cycle, respectively) to the cells at different SoH. Moreover, tests carried out on LIBs at different temperatures demonstrated that temperature effect on the implemented DWT-based method can be distinguished and separated from cycle aging effect. The proposed method allows a real-time SoH estimation showing a good accuracy (MAE, ME and RMSE respectively result in 0.917, 2.897 and 1.32) without requiring high computational efforts. This allows to assess battery SoH during the driving. The method can also be extended to other chemistries requiring a dedicated experimental activity for the parameters tuning.

Introduction

The recent directives on the climate change aim to accelerate the clean energy transition, taking part in the most polluting sectors, as the transportation sector. To reduce greenhouse gas emissions and pollutants, especially in urban areas, a massive electrification of the transports is expected.[1] In this context, Li-ion Batteries (LIBs) are used as on-board energy carrier to power electric light-weight vehicles, due to their high efficiency, fast response, high power and energy density and low self-discharge.[2,3] Such vehicles are defined battery electric vehicles (BEVs).

Nevertheless, major drawbacks related to the so-called "range anxiety" and the lack of fast charging infrastructure have to be addressed yet.[4]–[6] Moreover, LIBs are subject to degradation since the electrochemical reactions that take place within the cells are irreversible. Mechanical, electrical, and thermal factors, as the operating temperature, manufacturing inconsistency, charging and discharging C-rates, yield to a more or less fast cell degradation, which reflects in a capacity fade and an increase of the internal resistance.[3,7,8] Every BEV includes a battery management system (BMS) able to provide several information, including measured voltage and current, pack and cell temperature, and estimated capacity of the battery.[9] However, BMS generally has a low computational power and estimates battery State of Health (SoH) through simple methods, such as coulombic counting.[10,11] In addition, since LIB depth-of-discharge is usually limited for safety reasons in BEVs, BMS calculates battery SoH basing on partial charge and discharge cycles. This negatively affects the accuracy of the coulombic counting method. In general, EVs LIBs reach the end of life (EOL) once their capacity passes 80% of the initial value.[12] Therefore, without suitable monitor or prognostic solutions for cyclic capacity, both power and energy capabilities of a battery will drop fast.[13] Besides, the operational impairment and even catastrophic events can often occur during battery service period.[14]

Thus, an accurate real-time SoH prediction is essential to guarantee safety and reliability of a Li-ion battery. Generally, two main categories of SoH estimation can be distinguished: i) model-based and ii) data-driven methods.[15] In general, such methods aim to deeply predict the processes involving Li-ion battery cycle and calendar aging.[16] Specifically, in the view of the expected widespread of electric vehicles, several methodologies for LIB SoH estimation and remaining useful life (RUL) prediction have been widely investigated through suitable model-based approaches.[17–19]

With regards to data-driven methods, several studies are available in literature. Interesting works present approaches for battery performance monitoring[20] and RUL estimation.[21] Moreover, a BMS implementing multifrequency impedance real-time measurements[22] is developed to efficiently identify cell mismatches and emerging failures. Li-ion batteries calendar and cyclic aging prediction based on data-driven approach[13,23] is addressed by means of Gaussian process regression models. An online technique for SoH estimation of a Li-ion battery based

[a] Dr. D. Pelosi, Prof. L. Barelli
Department of Engineering
University of Perugia
Via G. Duranti, 93 06125 Perugia, Italy
E-mail: linda.barelli@unipg.it

[b] Dr. F. Gallorini, Dr. P. A. Ottaviano
VGA srl Via dell'Innovazione SNC,
06053 Deruta (PG), Italy

on a modified coulomb counting method[24] for solar photovoltaics systems is shown. An integrated framework of aging mechanisms and data-driven methods for Li-ion battery-accelerated aging diagnosis proved to be highly generic and accurate.[25] Different data-driven machine learning models[26] are presented to predict LIBs cycle life. However, such methods require high computation efforts and a great dataset for an accurate and reliable prediction not easily implementable in BMS and on-board diagnosis (OBD) systems. As mentioned above, since BMS in an EV has limited computational power, the use of computationally heavy methods, such as Kalman filters, neural networks, or fuzzy logic to calculate the degradation parameters of the Li-ion battery, is challenging.[10]

Several papers estimate LIB SoH by means of applying the discrete wavelet transform (DWT) directly to the measured voltage profile.[27–31] As matter of fact, the DWT is a powerful and easy-of-implement tool that facilitates the extraction of electrochemical features from signals with a broad frequency range through multi-resolution analysis. Anyway, the application of DWT on typical BEVs test drive cycles to predict Li-ion battery RUL is not presented in literature yet. Moreover, the temperature effect on DWT prediction for analysing EV battery SoH estimation has not yet been studied. Thus, with respect to literature, an innovative easy-of-implementation method for real-time SoH prediction and monitoring for EVs Li-ion batteries is presented in this paper. The method, based on the application of wavelet analysis to oscillating current profiles typical of BEVs operation, is proved to be accurate. Specifically, an extensive experimental campaign of cycle aging on NCR 18650 cells was performed, applying two typical US test drives (i.e., urban and extra urban drive cycle, respectively) to the tested cells at different SoH. Moreover, for the first time, the temperature effect on wavelet analysis is assessed demonstrating it can be easily distinguished from the one produced by cycle aging. Therefore, it is proved that such method allows a real-time SoH estimation showing a good accuracy (MAE, ME and RMSE are respectively assessed in 0.917, 2.897 and 1.32), taking into account the operating temperature, without requiring high computational efforts. At the best of our knowledge, such relevant aspects on DWT analysis applied to LIBs have not been treated in literature until now. This allows to predict LIB aging also during driving, continuously giving significant information to optimize battery exploitation over its lifespan. This also constitutes a relevant innovation with respect to current method based on coulombic counting, which needs the execution of a stationary full charge under controlled reference conditions (e.g., operating temperature, C-rates) to provide an accurate capacity assessment.

Due to the high innovative character of the obtained findings, main results of the present study have been reported in a patent application.[32]

The paper is organized as follows: Methodology section details the DWT theory and the implemented methodology, including the description of the experimental test rig and procedure. The main outcomes of this research work are illustrated in the Results and Discussion section, assessing both the aspects related to cycle aging and temperature effect on LIB voltage profiles by means of DWT analysis.

Methodology

In this section, an explanation of the DWT theory and the procedure for the experimental campaign is presented.

Theory and Application of the Wavelet Transform

Since LIB voltage is a non-stationary signal, the Fourier analysis is not effective because of the loss of the time information into the frequency domain passage.[33] Wavelet analysis allows to split a signal into shifted and scaled versions of the original wavelet.[34] The wavelet transform can be divided into continuous wavelet transform (CWT) and DWT. Nevertheless, CWT is unsuitable for the practical applications due to complex computation due to the high amount of data to be processed.[35] Therefore, DWT is generally used to reduce CWT complexity, decomposing the original signal in several resolutions. This makes it easier to examine the instantaneous variations of the analyzed signal in all the frequency bands. Such features allow the DWT technique to be widely used for systems diagnosis.[34] In other words, DWT divides the original signal into different time-frequency scales by means of digital filtering techniques. The signal passes through a series of high pass filters set at different cut-off frequencies to analyze the high frequencies, vice versa it goes through a series of low pass filters explore the low frequencies. These are the basis for the multi resolution analysis (MRA), since DWT enables the separation of the signal low frequency content from the high frequency one, representing to the detailed structure of the studied signal.[36]

Considering n decomposition levels, the wavelet function $\xi(t)$ and the scaling function $\vartheta(t)$ can be expressed as follows:

$$\xi_{j,n}(t) = 2^{\frac{j}{2}} \sum_{n} w_{j,n} \xi[2^j t - n] \tag{1}$$

$$\vartheta_{j,n}(t) = 2^{\frac{j}{2}} \sum_{n} u_{j,n} \vartheta[2^j t - n] \tag{2}$$

Where w_j and u_j are the scaling coefficient and the wavelet at scale j, respectively.

The MRA mathematical recursive representation can be defined as:[37]

$$V_j = W_{j+1} \oplus V_{j+1} = W_{j+1} \oplus \ldots \oplus W_{j+n} \oplus V_n \tag{3}$$

Where:

- V_{j+1} represents the approximate version of the original signal at scale $j+1$;
- W_{j+1} is the detailed version that includes all the original signal transient phenomena at scale $j+1$;
- n is the decomposition level;
- $\oplus$ denotes the summation of the two decomposed signals.

Assuming the original signal $x_j(t)$ at scale j is sampled at constant time intervals, i.e., $x_j(t) = (v_0, v_1, \ldots, v_{N-1})$, the sampling number corresponds to $N = 2^j$, where j is an integer number. For $x_j(t)$, its DWT equation is presented in eq. (4):

Research Article
doi.org/10.1002/batt.202300551
Chemistry Europe
European Chemical Societies Publishing

$$DWT(x_j(t)) = \sum_k x_j(t)\xi_{j,k}(t) =$$
$$> 2^{\frac{(j+1)}{2}}\left(\sum_n uA_{j+1,n}\xi[2^{j+1}t-n] + \sum_n wD_{j+1,n}\vartheta[2^{j+1}t-n]\right) \quad (4)$$
$$0 \le n \le \frac{N}{2^j} - 1$$

With:

$$uA_{j+1,n} = \sum_k c_{j,k}v_{j,k+2n} \quad (5)$$
$$0 \le k \le \frac{N}{2^j} - 1$$

$$wD_{j+1,n} = \sum_k w_{j,k}v_{j,k+2n} \quad (6)$$
$$0 \le k \le \frac{N}{2^j} - 1$$

$$d_k = (-1)^k c_{2p-1-k} \quad (7)$$
$$p = \frac{N}{2^j}$$

Where $uA_{j+1,n}$ and $wD_{j+1,n}$ are the approximate and the detailed versions at scale $j+1$.

Figure 1 shows the DWT basic decomposition and reconstruction view to different levels.

Specifically, the acquired signal x(t), constituted by N samples where $N=2^n$, goes through a high-pass filter, determining the wavelet coefficients at the shortest scale j. First, for $j=1$ the procedure performs the signal down-sampling. This generates an output signal with half length of the original one. The corresponding wavelet coefficients vector wD_1 has a length of 2n–1, as visible in Figure 1. Subsequently, the original signal x(t) is filtered with the low-pass filter: this process supplies the approximated coefficients vector uA_1 with length 2n–1. Finally, the process is repeated up to n=j.

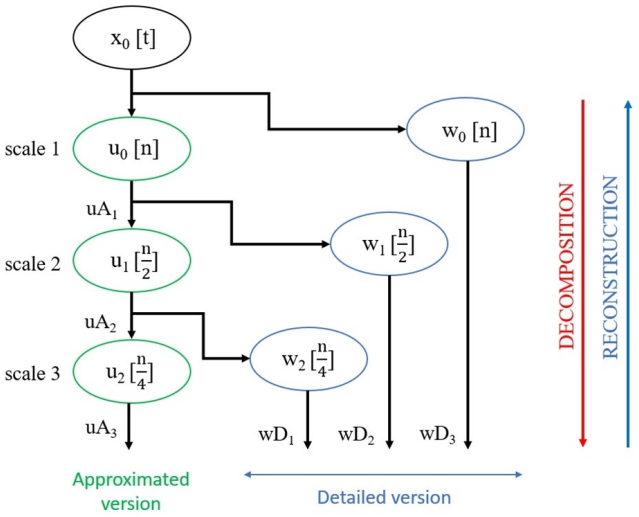

Figure 1. DWT basic decomposition and reconstruction view.

Finally, to extract the energy distribution of the analyzed signal through DWT, Parseval's theorem can be applied.[37] In Parseval's theorem, if a discrete signal x(n) is the current that flows through a resistive element, the energy of the resistance is equal to the square sum of the spectrum coefficients (a_k) of the Fourier transform in the frequency domain, according to eq. (8):

$$\frac{1}{N}\sum_{n=1}^{N}|x(n)|^2 = \sum_{n=1}^{N}|a_k|^2 \quad (8)$$

Where N represents the sampling period. Therefore, the Parseval's theorem representing the energy distribution of the signal in DWT can be expressed by eq. (9):

$$\frac{1}{N}\sum_t |x(t)|^2 = E_a + E_d =$$
$$\frac{1}{N_j}\sum_t |uA_{j,k}|^2 + \sum_{j=1}^{J}\left(\frac{1}{N_j}\sum_k |wD_{j,k}|^2\right) \quad (9)$$

Where E_a and E_d represent the average power of the approximated version and the detailed version of the decomposed signal, respectively.

BEV Test Drive profiles

To analyze the capacity fading over the time through DWT analysis, three different Li-ion cells were cycled, repeating two different drive cycles selected.[38] Specifically, the two drive tests are: the urban SC03 Test Drive, introduced by the Supplemental Federal Test Procedure (SFTP) to represent the engine load associated with use of air conditioning in vehicles certified over the FTP75 test cycle.[39] It corresponds to a mileage of 12.8 km at a maximum speed of 88.2 km/h and a duration of 596 seconds.

The extra urban SFTP-US06 Test Drive, representing the aggressive, high speed and/or high acceleration driving behavior, rapid speed fluctuations, and driving behavior following start-up.[40] It corresponds to a mileage of 12.8 km at a maximum speed of 129.2 km/h, with a duration of 596 seconds.

Figure 2 depicts the vehicle speed over the time for the considered test cycles and the related battery current profiles of the BEV.

Performance indicators

To assess the accuracy of the proposed technique, the deviation between the predicted values and the actual values is evaluated in terms of Mean Absolute Error (MAE), Maximum Absolute Error (ME) and Root-Mean-Square Error (RMSE). MAE indicator reveals the actual situations of the predicted errors. The larger the MAE, the less accurate the predicted results. ME reflects the maximum difference between the predicted values and the real values. The larger the ME, the bigger difference occurs during prediction. Otherwise, RMSE is used since it penalizes larger absolute values by giving them more weight. Such performance indicators are expressed according to eqs. (10)-(12):

$$MAE = \frac{1}{M}\sum_{i=1}^{M}|y_i - \hat{y}_i| \quad (10)$$

$$ME = \max_{1\le i\le M}|y_i - \hat{y}_i| \quad (11)$$

Research Article
doi.org/10.1002/batt.202300551
Chemistry Europe
European Chemical Societies Publishing

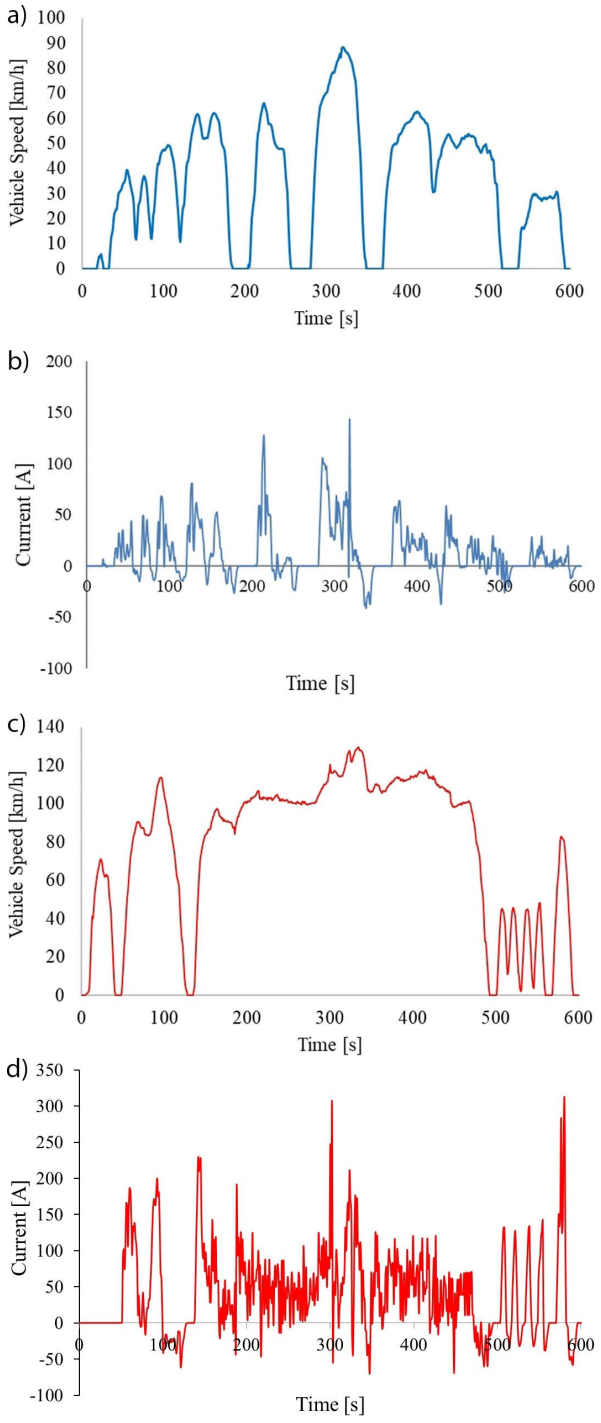

Figure 2. Vehicle speed vs. time (a,c) and battery current profile of the BEV (b,d), for the considered SC03 Test cycle (Fig. 2a, 2b) and US06 Test cycle (Fig. 2c, 2d).

$$RMSE = \sqrt{\frac{1}{M}\sum_{i=1}^{M}(y_i - \hat{y}_i)^2} \quad (12)$$

Where M denotes the total number of predictions, y_i and $\hat{y}_i$ represent the actual and the predicted values from the model, respectively.

Experimental Setup and Materials

The experimental campaigns were performed on Panasonic NCR 18650 Li-ion batteries, typically employed in BEVs.[41] The maximum continuous dis-/charge currents are respectively of 2 C and 0.7 C. A voltage range of 2.5-4.2 V was considered according to the safety limits imposed by manufacturer.[41] The maximum number of cycles was fixed at 300, since cell SoH overcomes the 80% threshold value, as indicated in the cycle aging tests performed by the manufacturer.

First, a cycle aging test was realized under 20±1 °C operating temperature to assess the actual cell degradation by means of coulombic counting method, evaluated according to the following procedure:

An initial battery capacity determination (BCD) was performed to determine the initial capacity of the fresh cell. BCD was carried out as follows: CC / CV charge (0.5 C / 4.2 V with a cut-off current of 65 mA) followed by a CC discharge (0.5 C).

Galvanostatic charge/discharge cycling at maximum C-rates (0.7 C charge; 2 C discharge) up to 300 cycles, with 5 minutes resting time between each charge and discharge. Every 30 cycles the following procedure was implemented:

1) after a full charge (up to 4.2 V) the extra urban US06 test drive cycle was applied and repeated until the achievement of the low voltage cut-off (2.5 V).
2) another full charge was performed, and the urban SC03 cycle applied up to the full discharge (achievement of the low voltage cut-off).
3) BCD technique was performed to assess battery capacity fading. BCD was carried out under same conditions of the initial assessment (0.5 C / 4.2 V with a cut-off current of 65 mA charge; 0.5 C discharge).

Figure 3 depicts the battery test rig. The galvanostat/potentiostat BioLogic® SP-300, connected to the tested cells through cable sensors, was used to perform the experiments.

In the second experimental campaign three NCR 18650 cells at different aging levels (i.e., new cell, 80% and 77% capacity respectively) were full charged and then discharged by applying

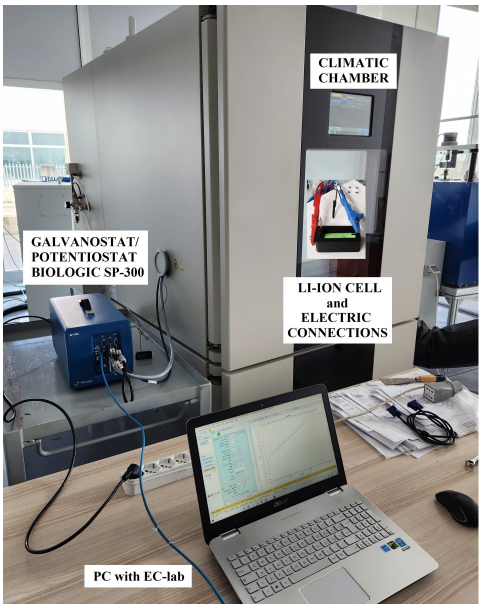

Figure 3. Test rig used for the experimental campaign.

repeatedly the US06 drive profile (up to the 2.5 V voltage cut-off) in a climatic chamber at three different operating temperatures: 0 °C and 30 °C, and the reference temperature of 20 °C. This to evaluate the variability of the wavelet analysis under the influence of temperature on voltage profiles.

Results and Discussion

In this section, the results gathered from the experimental campaign conducted on NCR 18650 cells are presented. Specifically, Section 4.1 illustrates the outcomes relating to the accelerated aging cycling interspersed with US06 and SC03 drive cycles at constant temperature of 20 ± 1 °C. Section 4.2 shows and discusses temperature and cycling aging impact on the internal resistance variation of the LIBs.

Cycling Analysis

The experimental voltage trends gathered from the tests were post-processed by means of DWT analysis in MATLAB environment. In the analysis here presented, the original signal was decomposed by using Daubechies basis of order three, in four decomposition levels.[29] As detailed in Table 1, the detail coefficients (D_1, D_2, D_3 and D_4) and the approximation A are analyzed according to the procedure described in Section 2. Specifically, it is emphasized as all the detail coefficients increase while the approximation decreases in magnitude consequently to the aging effect of the cell under cycling. A trend reversal can be distinguished around 120/150 cycles, indicating the non-linear behavior of the Li-ion chemistry during cycling.

Evaluating the percentage reduction of the details and approximation with respect to their previous values, it can be easily recognized with a good accuracy the capacity fading behavior of a LIB without any need of complex and elaborate models. This allows an easy implementation of wavelet for on-board diagnosis of the battery installed on BEVs only by acquiring the voltage signal during the drive. As matter of fact, the most used method for assessing the battery capacity on BEVs is based on coulombic cycling counting carried out during charging phase. Such method is very easy to implement in such applications but is not accurate. To be accurate it requires the execution of a full charge under reference and controlled conditions, as well as detailed measurement of the current. Moreover, it can be only applied when the vehicle is stopped for the charge.

Table 2 lists the percentage increase or decrease of the details and approximation with respect to the registered previous values.

As evident from Table 2, after a sudden increase of the details during the first 90 cycles, the behavior stabilizes. This reflects the typical capacity fading of a Li-ion battery under

Table 1. Main results of wavelet analysis in terms of details and approximation on the cycled NCR 18650 cylindrical cell at 20 °C (C_{meas} – measured capacity).

Cycles	C_{meas} (mAh)	D_1	D_2	D_3	D_4	A
0	3144	0.016	0.012	0.008	0.004	213.4
30	3116	0.018	0.013	0.009	0.004	211.9
60	3037	0.024	0.018	0.012	0.006	209.1
90	3027	0.033	0.025	0.017	0.008	206.5
120	2852	0.039	0.029	0.019	0.010	204.3
150	2803	0.032	0.024	0.016	0.008	206.6
180	2625	0.036	0.027	0.018	0.009	206.3
210	2602	0.035	0.026	0.017	0.009	206.3
240	2460	0.032	0.024	0.016	0.008	207.7

Table 2. Relative percentage difference of the details and the approximation with respect to the previous values for the considered NCR 18650 cylindrical cell (C_{red} – capacity reduction).

Cycles	C_{meas} (mAh)	C_{red} (%)	% D_1	% D_2	% D_3	% D_4	% A
0	3144	100.0%	–	–	–	–	–
30	3116	99.1%	13%	13%	13%	13%	−1%
60	3037	96.6%	35%	35%	35%	35%	−1%
90	3027	96.3%	41%	41%	41%	41%	−1%
120	2852	90.7%	15%	15%	15%	15%	−1%
150	2803	89.2%	−17%	−17%	−17%	−17%	1%
180	2625	83.5%	12%	12%	12%	12%	0%
210	2602	82.8%	-3%	-3%	-3%	-3%	0%
240	2460	78.2%	-9%	-9%	-9%	-9%	1%

Research Article
doi.org/10.1002/batt.202300551
Chemistry Europe
European Chemical Societies Publishing

cycling, highlighting a greater decrease in the first cycles losing more than 10% of the initial registered capacity and a subsequent reduced slope until the fixed EOL. Moreover, the reduction in terms of detail coefficients registered at 150 cycles emphasizes the battery capacity regeneration phenomena, reducing the efficiency of model-based predictive methods for RUL estimation.[42] This reflects the typical capacity fade behavior of a LIB, with a sudden and non-linear capacity reduction followed by a constant behavior.

By means of wavelet analysis, it can be found a correlation between detail coefficients, approximation and number of cycles realized by the Li-ion battery to analytically describe the capacity fading (C_{fade}). C_{fade} can be calculated as follows (eq. (13)):

$$C_{fade}(A, D_{1,4}, N) = \frac{A_0}{A_i}\, e^{-\left(\frac{1}{10}\frac{N_i}{A_i}\frac{\sum_{i}\sum_{n=1}^{4} D_{n,i}}{\sum_{n=1}^{4} D_{n,0}}\right)} * 100\ [\%] \quad (13)$$

Where A_i and A_0 are the approximation coefficients related to i-th aging cycle and to the fresh battery, respectively. N_i is the corresponding i-th number of cycles performed by the battery; $D_{n,0}$ and $D_{n,i}$ represent the detail coefficients at n levels for the new battery and after i cycles of aging. Figure 4 illustrates the predicted model described in eq. (13) and the actual measured data on the cycled NCR cell by means of BCD technique. It is emphasized the good accuracy of the model since the MAE, ME and RMSE are respectively assessed in 0.917, 2.897 and 1.32.

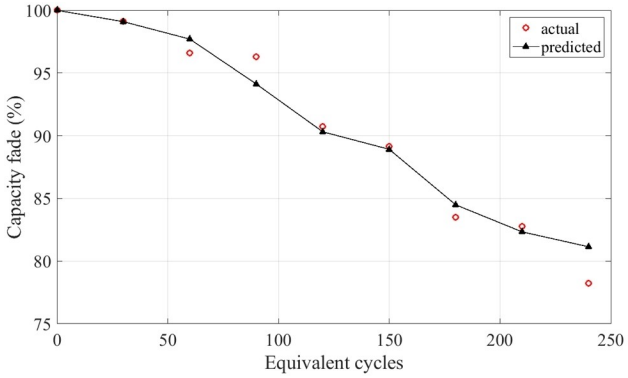

Figure 4. Predicted and actual capacity fading over cycling.

Temperature Effect on Wavelet Analysis

Temperature is a key factor involved in the electrochemical processes occurring in Li-ion batteries. Since temperature yields a significant effect on internal resistance variation which reflects in wider registered voltage amplitudes, its influence on new and aged LIB cells was studied. Specifically, three NCR 18650 cells at different aging levels (i.e., new cell, 80% and 77% capacity respectively) were tested in a climatic chamber. US06 drive profile was used for the experimental campaign. The outcomes of the wavelet analysis are listed in Table 3.

The percentage variations V_D and V_A with respect to the reference temperature T_{ref} (i.e., 20 °C), both in terms of detail coefficients D and the approximation A, are evaluated as follows:

$$V_{D_n} = \frac{Dn_T - Dn_{T_{ref}}}{Dn_{T_{ref}}}\ [\%] \quad (14)$$

$$V_A = \frac{A_T - A_{T_{ref}}}{A_{T_{ref}}}\ [\%] \quad (15)$$

Where Dn_T and A_T represent the values of the detail coefficient at n level and the approximation at temperature T and $Dn_{T_{ref}}$ and $A_{T_{ref}}$ the values of the detail coefficient at n level and the approximation at the reference temperature T_{ref}. Table 4 lists the temperature effect in terms of V_{D_n} and V_A on details and approximation for each tested cell and the mean values among the three cells. V_{D_n} index, with values equal for all the details at a fixed temperature, reduces when temperature rises, while V_A shows an opposite trend. V_{D_n} values are in a narrow range at a fixed temperature whatever is the cell aging; the same is for V_A values, highlighting that the dependence of V_{D_n} and V_A on the cycle aging can be neglected, if compared to the strong dependence on the operating temperature. Consequently, by applying DWT analysis, temperature effect on LIBs aging can be easily distinguished from the one produced by cycle aging. This demonstrates the effectiveness of the

Table 3. Details and approximation coefficients at different temperatures and aging levels.

NCR cell	C (%)	T (°C)	D_1	D_2	D_3	D_4	A
Fresh	100	30	0.011	0.009	0.006	0.003	213.53
		20	0.016	0.012	0.008	0.004	213.39
		0	0.039	0.030	0.020	0.010	207.80
Aged 1	80	30	0.021	0.016	0.010	0.005	210.07
		20	0.029	0.022	0.015	0.007	210.85
		0	0.070	0.053	0.035	0.018	205.11
Aged 2	77	30	0.019	0.014	0.010	0.005	216.23
		20	0.032	0.024	0.016	0.008	207.74
		0	0.102	0.076	0.051	0.025	195.68

Research Article
doi.org/10.1002/batt.202300551
Chemistry Europe
European Chemical Societies Publishing

Table 4. Percentage variations for the detail coefficients and approximation with respect to the reference case (20 °C) for each tested cell and the mean values over the three cells.

NCR cell	C (%)	T (°C)	V_{D_1}	V_{D_2}	V_{D_3}	V_{D_4}	V_A
Fresh	100	30	−27%	−27%	−27%	−27%	0%
		20	–	–	–	–	–
		0	154%	154%	154%	154%	−3%
Aged 1	80	30	−29%	−29%	−29%	−29%	0%
		20	–	–	–	–	–
		0	139%	139%	139%	139%	−3%
Aged 2	77	30	−39%	−39%	−39%	−39%	4%
		20	–	–	–	–	–
		0	221%	221%	221%	221%	−6%
Mean value		30	−32%	−32%	−32%	−32%	1%
		20	–	–	–	–	–
		0	155%	155%	155%	155%	−3%

proposed method in online assessment of battery capacity fading in BEVs applications. This is due to the great ability of DWT-based analysis to extract variable information of electrochemical characteristics from the non-stationary and transient phenomena in both the time and frequency domains.[43]

Conclusions

Since SoH evaluation is of crucial prominence in extending EV LIB lifespan, several data-driven and model-based methods are illustrated in scientific literature. Nevertheless, although machine learning and neural network approach provides the best results in terms of SoH prediction, managing a great amount of data requires high computational efforts and time. This aspect slows their implementation in BEVs BMS and OBD systems. Hence, applying an accurate and easy-of-implement technique to predict LIBs RUL is of utmost importance to extend battery lifespan. With this purpose, an online DWT-based prediction method for Li-ion battery RUL is shown in this paper. Specifically, an extensive experimental campaign of cycle aging on NCR 18650 cells was performed, applying two typical US test drives (i.e., urban and extra urban drive cycle, respectively) to the tested cells at different SoH. Moreover, several tests carried out at different temperatures on DWT analysis demonstrate that the temperature effect on LIBs voltage profiles can be distinguished and separated. Therefore, it is proved that such method allows a real-time SoH estimation showing a good accuracy (MAE, ME and RMSE are respectively assessed in 0.917, 2.897 and 1.32) without requiring high computational efforts. This allows to predict LIB aging during the driving as well, without requiring stationary full charge under reference conditions and giving continuously significant information.

Conflict of Interests

The authors declare no conflict of interest.

Data Availability Statement

The data that support the findings of this study are available from the corresponding author upon reasonable request.

Keywords: cycle aging · discrete wavelet transform · Li-ion Battery · multi resolution analysis · state of health estimation

[1] L. Barelli, D. Pelosi, M. Longo, D. Zaninelli, in *2022 IEEE Power & Energy Society General Meeting (PESGM)*, IEEE, Denver, CO, USA, **2022**, pp. 01–05.
[2] X. Wang, X. Wei, J. Zhu, H. Dai, Y. Zheng, X. Xu, Q. Chen, *eTransportation* **2021**, *7*, 100093.
[3] X. Han, L. Lu, Y. Zheng, X. Feng, Z. Li, J. Li, M. Ouyang, *eTransportation* **2019**, *1*, 100005.
[4] A. Tomaszewska, Z. Chu, X. Feng, S. O'Kane, X. Liu, J. Chen, C. Ji, E. Endler, R. Li, L. Liu, Y. Li, S. Zheng, S. Vetterlein, M. Gao, J. Du, M. Parkes, M. Ouyang, M. Marinescu, G. Offer, B. Wu, *eTransportation* **2019**, *1*, 100011.
[5] A. Saldarini, L. Barelli, D. Pelosi, S. Miraftabzadeh, M. Longo, W. Yaici, in *2022 IEEE International Conference on Environment and Electrical Engineering and 2022 IEEE Industrial and Commercial Power Systems Europe, EEEIC / I and CPS Europe 2022*, Institute Of Electrical And Electronics Engineers Inc., **2022**.
[6] D. Pelosi, M. Longo, G. Bidini, D. Zaninelli, L. Barelli, *J. Energy Storage* **2023**, *65*, Doi: 10.1016/j.est.2023.107364.
[7] Z. Song, X. G. Yang, N. Yang, F. P. Delgado, H. Hofmann, J. Sun, *eTransportation* **2021**, *7*, 100091.
[8] C. Vidal, O. Gross, R. Gu, P. Kollmeyer, A. Emadi, *IEEE Trans. Veh. Technol.* **2019**, *68*, 4560–4572.
[9] L. Calearo, C. Ziras, A. Thingvad, M. Marinelli, *Energies* **2022**, *15*, 9656.
[10] A. Thingvad, L. Calearo, P. B. Andersen, M. Marinelli, *IEEE Trans Veh Technol* **2021**, *70*, 7547–7557.
[11] H. Hamed, M. Yusuf, M. Suliga, B. Ghalami Choobar, R. Kostos, M. Safari, *Batter Supercaps* **2023**, *6*, Doi: 10.1002/batt.202300140.
[12] Y. Z. Zhang, R. Xiong, H. W. He, X. Qu, M. Pecht, *eTransportation* **2019**, *1*, 100004.
[13] K. Liu, X. Hu, Z. Wei, Y. Li, Y. Jiang, *IEEE Transactions on Transportation Electrification* **2019**, *5*, 1225–1236.
[14] A. Barré, B. Deguilhem, S. Grolleau, M. Gérard, F. Suard, D. Riu, *J. Power Sources* **2013**, *241*, 680–689.
[15] M. Elmahallawy, T. Elfouly, A. Alouani, A. Massoud, *IEEE Access* **2022**, *10*, 1–1.
[16] T. Raj, A. A. Wang, C. W. Monroe, D. A. Howey, *Batter Supercaps* **2020**, *3*, 1377–1385.

[17] E. Chiodo, P. De Falco, L. P. Di Noia, *IEEE Trans. Ind. Appl.* **2022**, *58*, 5214–5226.
[18] Z. Lyu, R. Gao, L. Chen, *IEEE Trans Power Electron* **2021**, *36*, 6228–6240.
[19] T. Aggab, M. Avila, P. Vrignat, F. Kratz, *IEEE Syst J* **2021**, *15*, 5245–5254.
[20] H. M. Khalid, Q. Ahmed, J. C. H. Peng, G. Rizzoni, *IEEE Transactions on Transportation Electrification* **2015**, *1*, 402–412.
[21] K. Liu, Y. Shang, Q. Ouyang, W. D. Widanage, *IEEE Transactions on Industrial Electronics* **2021**, *68*, 3170–3180.
[22] B. G. Carkhuff, P. A. Demirev, R. Srinivasan, *IEEE Transactions on Industrial Electronics* **2018**, *65*, 6497–6504.
[23] K. Liu, Y. Li, X. Hu, M. Lucu, W. D. Widanage, *IEEE Trans Industr Inform* **2020**, *16*, 3767–3777.
[24] J. S. Goud, R. Kalpana, B. Singh, *IEEE Transactions on Energy Conversion* **2021**, *36*, 111–119.
[25] X. Jia, C. Zhang, L. Y. Wang, L. Zhang, X. Zhou, *IEEE Transactions on Transportation Electrification* **2022**, *8*, 4722–4742.
[26] L. Su, M. Wu, Z. Li, J. Zhang, *eTransportation* **2021**, *10*, 100137.
[27] C. Zhang, Y. He, L. Yuan, S. Xiang, J. Wang, **2015**, Doi: 10.1155/2015/918305.
[28] P. Ding, X. Liu, H. Li, Z. Huang, K. Zhang, L. Shao, O. Abedinia, *Renewable Sustainable Energy Rev.* **2021**, *148*, 111287.
[29] Y. Wang, R. Pan, D. Yang, X. Tang, Z. Chen, *Energy Procedia* **2017**, *105*, 2053–2058.
[30] M. S. Park, J. K. Lee, B. W. Kim, *Applied Sciences 2022, Vol. 12, Page 3996* **2022**, *12*, 3996.
[31] Z. L. Zhang, X. Cheng, Z. Y. Lu, D. J. Gu, *IEEE Trans Power Electron* **2017**, *32*, 7626–7634.
[32] L. Barelli, D. Pelosi, F. Gallorini, A. P. Ottaviano, *Metodo per Valutare Lo Stato Di Salute Di Una Batteria Elettrica Agli Ioni Di Litio*, 102023000017487.
[33] J. Kim, B. H. Cho, *J. Power Sources* **2014**, *260*, 115–130.
[34] L. Barelli, E. Barluzzi, G. Bidini, F. Bonucci, *Appl. Energy* **2012**, *92*, 44–50.
[35] C. A. Naik, P. Kundu, *International Journal of Electrical Power and Energy Systems* **2013**, *53*, 994–1002.
[36] J. Da Wu, C. K. Huang, Y. W. Chang, Y. J. Shiao, *Expert Syst Appl* **2010**, *37*, 949–958.
[37] Z. L. Gaing, *IEEE Trans. Power Delivery* **2004**, *19*, 1560–1568.
[38] S. Barcellona, M. Brenna, F. Foiadelli, M. Longo, L. Piegari, in *2015 IEEE 1st International Forum on Research and Technologies for Society and Industry Leveraging a Better Tomorrow (RTSI)*, **2015**, pp. 6–10.
[39] "US: Light-duty SC03 Test," can be found under https://www.transport-policy.net/standard/us-light-duty-sc03-test/.
[40] "Emission Test Cycles: SFTP-US06," can be found under https://dieselnet.com/standards/cycles/ftp us06.php.
[41] Panasonic, "Panasonic NCR18650B," can be found under https://asset.conrad.com/media10/add/160267/c1/-/en/001436402DS01/scheda-tecnica-1436402-panasonic-ncr18650b-batteria-ricaricabile-speciale-18650-li-ion-37-v-3400-mah.pdf.
[42] Z. X. Yang, G. Yu, J. Zhao, P. K. Wong, X. B. Wang, *IEEE Trans. Veh. Technol.* **2021**, *70*, 6613–6625.
[43] J. Kim, *IEEE Trans. Veh. Technol.* **2016**, *65*, 1150–1161.

Manuscript received: November 24, 2023
Revised manuscript received: February 12, 2024
Accepted manuscript online: February 18, 2024
Version of record online: March 4, 2024